INQUA Focus Group Earthquake Geology and Seismic Hazards

paleoseismicity.org

Three-dimensional coastal deformation in the M_w 7.8 Kaikōura earthquake from differential airborne lidar

Nissen, Edwin (1), Malireddi, Sri Raghu (2), Clark, Kate (3), Hamling, Ian (3), Langridge, Robert (3), Ries, William (3), and Tagliasacchi, Andrea (2)

(1) School of Earth and Ocean Sciences, University of Victoria, Victoria BC, Canada. enissen@uvic.ca.
(2) Department of Computer Science, University of Victoria, Victoria BC, Canada
(3) GNS Science, PO Box 30368, Lower Hutt 5040, New Zealand

Abstract: *We investigate coastal deformation in the 2016 Mw 7.8 Kaikōura earthquake by differencing airborne lidar topography data surveyed in 2012 and late 2016. The 90 km-long, 1 km-wide strip of lidar double-coverage crosses coastal outcrops of the Hundalee, Hope, Papatea and Kekerengu faults, and also extends inland for several kilometers along the Papatea fault. We compute the three-dimensional coseismic surface displacement field using new adaptations of the Iterative Closest Point algorithm. Resulting surface displacements are in good agreement with independent measurements, but with better spatial coverage (over field and GPS data) and improved coherence (over InSAR). We observe multiple-wavelength signals related to oblique rupture of shallow upper plate faults, off-fault deformation, and possibly slip on the underlying plate interface. The complex coastal uplift pattern should prompt reassessment of coastal paleoseismic and marine terrace records that may not have considered multiple-fault ruptures of this type.*

Key words*: Lidar, coseismic surface deformation, Kaikōura earthquake*

INTRODUCTION

The 13 November 2016 M_w 7.8 Kaikōura (New Zealand) earthquake cascaded across a fractured array of onshore and offshore reverse, strike-slip and oblique-slip faults within the Marlborough Fault System (Hamling *et al.,* 2017). At least twenty distinct faults are known to have slipped coseismically (Stirling *et al.,* 2017), making this one of the most complicated earthquakes on record globally. These faults mark the transition between westward subduction of Pacific oceanic lithosphere beneath the North Island, and continental strike-slip along the Alpine Fault in the South Island (Wallace *et al.,* 2012). The Kaikōura earthquake therefore offers insights both into the rupture process of a major, multi-segmented earthquake and into the regional fault kinematics.

The Kaikōura earthquake was well-recorded by field surveys (Clark *et al.,* 2017; Stirling *et al.,* 2017), by satellite optical sub-pixel correlation (Hollingsworth *et al.,* 2017; Kääb *et al.,* 2017) and InSAR (Hamling *et al.,* 2017), and by regional and teleseismic seismometers (Bai *et al.,* 2017; Duputel & Rivera, 2017; Kaiser *et al.,* 2017; Zhang *et al.,* 2017). However, due in part to the complexity of the surface deformation and seismic wave fields, the relative importance of the constitutive faults and their geometries at depth remain uncertain. In particular, the presence or absence of coseismic slip on the southernmost Hikurangi subduction megathrust has been subject to much debate (e.g. Bai *et al.,* 2017; Furlong & Herman, 2017; Hamling *et al.,* 2017; Clark *et al.,* 2017). Whether or not rupture segments with disconnected surface traces are linked at depth is of general importance for understanding of how earthquakes propagate and terminate (e.g. Wesnousky, 2006; Nissen *et al.,* 2016). This question is of fundamental significance to the field of paleoseismology, since it informs how to interpret overlapping paleo-earthquake ages from trench sites on neighbouring but distinct faults.

The aim of this project is to provide additional constraints on source faulting in the Kaikōura earthquake using paired airborne lidar surveys undertaken in 2012, four years before the earthquake, and in late 2016, during the weeks after it. By mapping topography at a finer (sub-meter) spatial resolution than coseismic slip (up to several meters in this earthquake), lidar has the potential for revealing details of the earthquake that satellite-based imaging may have overlooked. However, to our knowledge this is only the seventh earthquake globally, and the first coastal event, to be captured (to any extent) with "before" and "after" lidar topography, and methodologies for differencing high-resolution topographic datasets are still in a nascent phase (e.g. Leprince *et al.,* 2011; Borsa & Minster, 2012; Oskin *et al.,* 2012; Nissen *et al.,* 2012). An additional motivation of ours is therefore to use the Kaikōura earthquake as a test case for improving the ways in which repeat topography data are analyzed.

METHODS

The Kaikōura coastline was mapped with airborne lidar in July 2012 and again in the weeks following the earthquake, providing a narrow (ca. 0.5 – 4 km), ca. 90 km-long coastal strip of repeat, sub-meter resolution topography. Details of the two surveys are provided in Clark *et al.* (2017). In this updated analysis, we additionally exploit newly-available lidar double coverage inland of the coastline along the lower Clarence River valley, capturing much of the Papatea fault rupture.

We applied two complementary approaches to mapping the surface deformation. Initially, we were most interested in deciphering the vertical component of deformation. The most convenient method for doing so is to subtract digital elevation models of the 2012 lidar survey from those of the 2016 survey (a "DEM of Difference"). This is also the most computationally-manageable approach – since it relies

only upon regularly-gridded (rasterized) data – and furthermore it can be undertaken at close to the full resolution of the lidar data. However, a key limitation is that lateral motions are neglected; raw elevation changes are influenced by horizontal displacement magnitude and azimuth, slope aspect and angle, and topographic roughness, all of which can obscure the true vertical deformation signal (Oskin *et al.,* 2012; Duffy *et al.,* 2013).

However, restricting the calculations to flat, smooth parts of the topography greatly reduces such biasing, such that the simple elevation change closely resembles the true vertical displacement (Clark *et al.,* 2017). Therefore, we restricted the DoD calculations to areas with slopes of <5°. Because our focus is on coseismic displacements, rather than erosional or depositional processes, we also removed riverbeds, beaches and landslides from the analysis. Finally, we also found that applying an additional cut-off in surface area further enhanced the signal-to-noise, reducing localized scatter in elevation changes to typically ca. 1 m for areas of <10 m^2, and ca. 0.5 m for larger areas of <2000 m^2.

In the second approach, we compute the three-dimensional coseismic surface displacement field through local registrations (alignments) of the 2012 and 2016 lidar point clouds. This has the obvious advantage of accounting fully, and equitably, for the three components of the deformation field, but comes at the expense of spatial resolution, since the datasets must be correlated over an area that greatly exceeds the raw lidar point spacing. Working well with irregular point clouds, this approach is truest to the original data but also challenging computationally.

Various algorithms have been proposed to determine three-dimensional deformation from repeat topographic data (Leprince *et al.,* 2011; Borsa & Minster, 2012; Nissen *et al.,* 2012; Zhang *et al.,* 2015; Moya *et al.,* 2017). We develop and apply our own adaptation of the Iterative Closest Point (ICP) point cloud registration algorithm (Besl & McKay, 1992; Chen & Medioni, 1992), building upon previous work by Nissen *et al.* (2012, 2014) and Glennie *et al.* (2014). The pre- and post-earthquake point clouds are first filtered to remove vegetation and building laser returns, and then split into overlapping square cells. Each pre-earthquake cell is then aligned with its equivalent post-event cell by minimizing closest neighbour distances, through an iterative sequence of rigid body translations along and rotations about the *x* (North-South), *y* (East-West) and *z* (up-down) coordinate axes. For each pair of cells, the summed translation over all iterations defines the local coseismic surface displacement; repeated across the entire scene, the displacement field is mapped.

We explored various implementations of ICP, including point-to-point and point-to-plane varieties as well as a new "sparse ICP" approach that iteratively re-weights the point clouds to lend greater prominence to those points which held more influence during the previous iteration (Bouaziz *et al.,* 2013). The iterative re-weighting acts to reduce the influence of outlier points, which can otherwise potentially lead regular ICP towards local, rather than global, minima in the registration misfit. After trial and error, we find that 50 m-wide cells provide the best balance of high spatial resolution and displacement robustness. However, we also implement a "sliding window" option that allows additional densification of the displacement field.

Our ICP approach is implemented within a single MATLAB script and requires no other dependencies, and is available upon request to the authors.

RESULTS

Elevation change results are plotted on a SW – NE-oriented line of projection that approximately parallels the Kaikōura coastline (Figure 1a, reproduced from Clark *et al.,* 2017). We discuss the elevation change profile at length in Clark *et al.* (2017), and provide only a brief summary of our observations below.

Several interesting trends are apparent. Abrupt vertical offsets related to slip on the Hundalee fault (Figure 1b) and the double-stranded Papatea fault (Figure 1d) are clear, though we observe no such displacement across the Hope fault. Broader (ca. 10 km length scale) swells of uplift northeast of the Hundalee fault and southwest of the Papatea fault are probably related to slip at depth on these faults. Highly localized (200 – 400 m length scale) subsidence of up to ca. 3 m around the Kekerengu fault is harder to interpret, as it occurs on both sides of the fault (Figure 1a). This may be related to bulk material processes such as fault zone dilatancy rather than elastic slip on the Kekerengu fault, which would give rise to a much broader displacement pattern.

A broad swell of uplift is observed from ca. 4 km south to ca. 16 km north of the Kaikōura Peninsula (Figure 1a), and the peninsula itself appears to have been tilted slightly towards the NW (Figure 1c). These signals do not appear related to any of the faults that cross the area of lidar double coverage, and marine surveying indicates that the Hundalee fault rupture probably terminates south of the peninsula (Clark *et al.,* 2017). The signal appears too abrupt to be explained by slip on the subduction interface, which is at ca. 19 km depth in this area. We tentatively ascribe this deformation to slip on an offshore reverse fault that strikes SW and dips ca. 35° beneath Kaikōura peninsula. Slip on this structure may be responsible for the ca. 2 m sea level draw-down observed on a tide gauge at Kaikōura over ca. 24 minutes after the earthquake.

An example of our three-dimensional deformation measurements is shown in Figure 2, from along a section of the Papatea fault rupture in the Clarence River valley.

INQUA Focus Group Earthquake Geology and Seismic Hazards

paleoseismicity.org

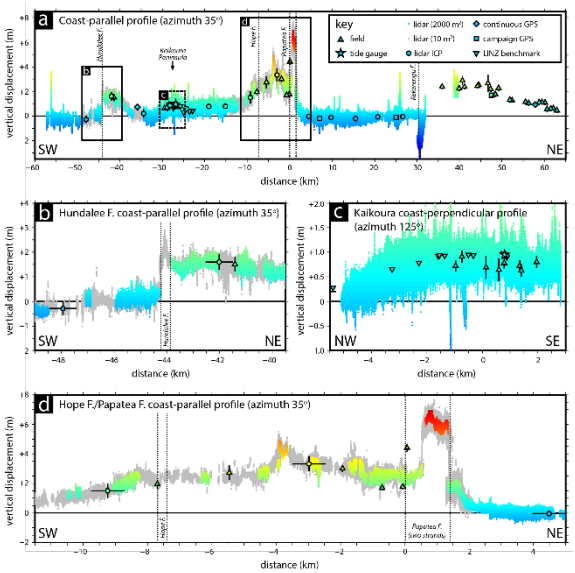

Figure 1: reproduced from Clark et al. (2017). (a) Elevation changes projected onto a 35°-trending straight line which parallels the Kaikōura coastline. The profile is centered (x = 0) at the Papatea fault and vertical dashed lines mark locations of major faults at the coastline. Vertical bars show 95% confidence bounds on field coastal uplift measurements and GPS-derived vertical displacements (the latter are barely visible at this scale). Coloured points represent elevation changes calculated from overlapping surface areas >2000 m^2; the grey points represent surface areas >10 m^2. (b) Detail across the Hundalee fault. (c) Coastline-perpendicular uplift profile (azimuth 125°, projection center at Kaikōura township) showing tilting across the Kaikōura Peninsula. (d) Detail across the Hope and Papatea faults.

Spurious ICP results, caused by changes to internal cell topography such as along the Clarence River, have been filtered from the figure. Work towards reproducing the full displacement field is ongoing, reflecting in part the computational challenge of manipulating very large point cloud datasets (hundreds of gigabytes).

Left-lateral and vertical offsets across the Papatea rupture are clearly resolved in the displacement field. A parallel strand of faulting around ca. 1 km west of the Papatea fault can also be observed, upthrown to the east and with a small left-lateral component. Furthermore, *absolute* motions of the two sides of the Papatea fault can be determined. The block west of it moved several meters southwards and upwards, whereas the block east of it remained relatively stationary, moving only a little towards the west (in good agreement with coarser-resolution SAR pixel offset results; Hamling *et al.,* 2017).

Displacement vectors appear remarkably consistent even around the highly-sinuous trace of the rupture. This implies that the slip vector is quite constant even as the style of faulting changes around the fault bends. In the northwest part of the scene, the NW-SE-trending scarp accommodates left-lateral strike-slip with very little fault-normal motion (despite the clear vertical offset). In the southeast part of the scene, the N-S-trending scarp accommodates roughly equal amounts of left-lateral strike-slip and shortening.

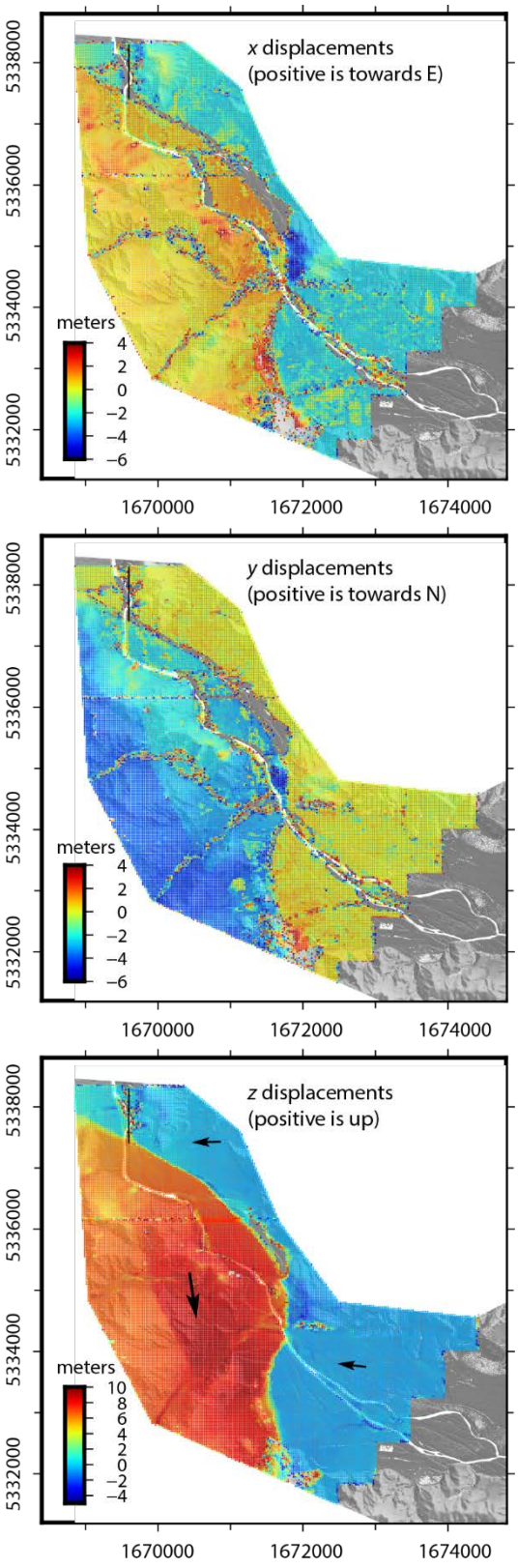

Figure 2: ICP results from part of the Papatea fault, using a cell size of 50 m, a slide of 25 m, and point-to-plane ICP. The panels show E-W, N-S and up-down displacements, respectively. The general sense of the horizontal motions is shown on the final panel by black arrows. Coordinates are given in meters in the NZTM2000 coordinate system.

INQUA Focus Group Earthquake Geology and Seismic Hazards

paleoseismicity.org

Acknowledgements: We thank Land Information New Zealand, New Zealand Transport Authority, Environment Canterbury, Marlborough District Council, Aerial Surveys Ltd and AAM NZ Ltd for providing excellent lidar data. The 2012 lidar data (http://dx.doi.org/10.5069/G98C9T67) and derived products are hosted and disseminated by the OpenTopography Facility (http://www.opentopography.org/) with support from the US National Science Foundation under NSF Awards #1226353 and #1225810. E.N. and S.R.M. were supported by the Natural Sciences and Engineering Research Council of Canada (NSERC) through Discovery Grant #2017-04029.

REFERENCES

Bai, Y., Lay, T., Cheung, K. F., & Ye, L., 2017. Two regions of seafloor deformation generated the tsunami for the 13 November 2016, Kaikoura, New Zealand earthquake. *Geophysical Research Letters* 44, 6597–6606.

Besl, P. J., & McKay, N. D., 1992. A method for registration of 3-D shapes. *IEEE Transactions on Pattern Analysis and Machine Intelligence* 14 (2), 239-256.

Borsa, A., & Minster, J. B., 2012. Rapid Determination of near-fault earthquake deformation using differential LiDAR. *Bulletin of the Seismological Society of America* 102 (4), 1335-1347.

Bouaziz, S., Tagliasacchi, A., & Pauly, M., 2013, Sparse Iterative Closest Point. *Computer Graphics Forum* 32, 113–123.

Chen, Y., & Medioni, G., 1992. Object modelling by registration of multiple range images. *Image and Vision Computing* 10 (3), 145-155.

Clark, K. J., Nissen, E. K., Howarth, J. D., Hamling, I. J., Mountjoy, J. J., Ries, W. F., Hreinsdóttir, S., Litchfield, N. J., Mueller, C., Berryman, K. R., & Strong, D. T., 2017. Highly variable coastal deformation in the 2016 M_w 7.8 Kaikōura earthquake reflects rupture complexity along a transpressional plate boundary. *Earth and Planetary Science Letters* 474, 334-344.

Duffy, B., Quigley, M., Barrell, D. J., Van Dissen, R., Stahl, T., Leprince, S., McInnes, C., & Bilderback, E., 2013. Fault kinematics and surface deformation across a releasing bend during the 2010 M_w 7.1 Darfield, New Zealand, earthquake revealed by differential LiDAR and cadastral surveying. *Geological Society of America Bulletin* 125 (3-4), 420-431.

Duputel, Z., & Rivera, L., 2017. Long-period analysis of the 2016 Kaikoura earthquake. *Physics of the Earth and Planetary Interiors* 265, 62-66.

Fielding, E. J., Lundgren, P. R., Bürgmann, R., & Funning, G. J., 2009. Shallow fault-zone dilatancy recovery after the 2003 Bam earthquake in Iran. *Nature* 458 (7234), 64-68.

Furlong, K. P., & Herman, M., 2017. Reconciling the Deformational Dichotomy of the 2016 M_w 7.8 Kaikoura NZ Earthquake. *Geophysical Research Letters* 44, 6788–6791.

Glennie, C. L., Hinojosa-Corona, A., Nissen, E., Kusari, A., Oskin, M. E., Arrowsmith, J. R., & Borsa, A., 2014. Optimization of legacy lidar data sets for measuring near-field earthquake displacements. *Geophysical Research Letters* 41 (10), 3494-3501.

Hamling, I. J., Hreinsdóttir, S., Clark, K., Elliott, J., Liang, C., Fielding, E., Litchfield, N., Villamor, P., Wallace, L., Wright, T. J., D'Anastasio, E., Bannister, S., Burbidge, D., Denys, P., Gentle, P., Howarth, J., Mueller, C., Palmer, N., Pearson, C., Power, W., Barnes, P., Barrell, D. J. A., Van Dissen, R., Langridge, R., Little, T., Nicol, A., Pettinga, J., Rowland, J., & Stirling, M., 2017. Complex multifault rupture during the 2016 Mw 7.8 Kaikōura earthquake, New Zealand. *Science* 356 (6334), eaam7194.

Hollingsworth, J., Ye, L., & Avouac, J. P., 2017. Dynamically triggered slip on a splay fault in the Mw 7.8, 2016 Kaikoura (New Zealand) earthquake. *Geophysical Research Letters* 44, 3517-3525.

Kääb, A., Altena, B., & Mascaro, J., 2017. Coseismic displacements of the 14 November 2016 M_w 7.8 Kaikoura, New Zealand, earthquake using the Planet optical cubesat constellation, *Natural Hazards and Earth Systems Sciences* 17, 627-639.

Kaiser, A., Balfour, N., Fry, B., Holden, C., Litchfield, N., Gerstenberger, M., D'Anastasio, E., Horspool, N., McVerry, G., Ristau, J., Bannister, S., Christophersen, A., Clark, K., Power, W., Rhoades, D., Massey, C., Hamling, I., Wallace, L., Mountjoy, J., Kaneko, Y., Benites, R., Van Houtte, C., Dellow, S., Wotherspoon, L., Elwood, K., Gledhill K., & Bannister, S., 2017. The 2016 Kaikōura, New Zealand, Earthquake: Preliminary Seismological Report. *Seismological Research Letters* 88 (3), 727-739.

Leprince, S., Hudnut, K. W., Akciz, S. O., Hinojosa-Corona, A., & Fletcher, J. M., 2011. Surface rupture and slip variation induced by the 2010 El Mayor—Cucapah earthquake, Baja California, quantified using COSI-Corr analysis on pre-and post-earthquake lidar acquisitions. *American Geophysical Union Fall Meeting*, EP41A-0596.

Moya, L., Yamazaki, F., Liu, W., & Chiba, T., 2017. Calculation of coseismic displacement from lidar data in the 2016 Kumamoto, Japan, earthquake. *Natural Hazards and Earth System Sciences* 17 (1), 143-156.

Nissen, E., Krishnan, A. K., Arrowsmith, J. R., & Saripalli, S., 2012. Three-dimensional surface displacements and rotations from differencing pre-and post-earthquake LiDAR point clouds. *Geophysical Research Letters* 39, L16301.

Nissen, E., Maruyama, T., Arrowsmith, J. R., Elliott, J. R., Krishnan, A. K., Oskin, M. E., & Saripalli, S., 2014. Coseismic fault zone deformation revealed with differential LiDAR: Examples from Japanese M_w ~7 intraplate earthquakes. *Earth and Planetary Science Letters* 405, 244-256.

Nissen, E., Elliott, J. R., Sloan, R. A., Craig, T. J., Funning, G. J., Hutko, A., Parsons, B. E., & Wright, T. J., 2016. Limitations of rupture forecasting exposed by instantaneously triggered earthquake doublet. *Nature Geoscience* 9 (4), 330-336.

Oskin, M. E., Arrowsmith, J. R., Corona, A. H., Elliott, A. J., Fletcher, J. M., Fielding, E. J., Gold, P. O., Gonzalez Garcia, J. J., Hudnut, K. W., Liu-Zeng, J., & Teran, O. J., 2012. Near-field deformation from the El Mayor–Cucapah earthquake revealed by differential LIDAR. *Science* 335 (6069), 702-705.

Stirling, M. W., and fifty-seven others, 2017. The M_w 7. 8 2016 Kaikōura earthquake: Surface fault rupture and seismic hazard context. *Bulletin of the New Zealand Society for Earthquake Engineering* 50 (2), 73-84.

Wallace, L. M., Barnes, P., Beavan, J., Van Dissen, R., Litchfield, N., Mountjoy, J., Langridge, R., Lamarche, G., & Pondard, N., 2012. The kinematics of a transition from subduction to strike-slip: An example from the central New Zealand plate boundary. *Journal of Geophysical Research: Solid Earth* 117, B02405.

Wesnousky, S. G., 2006. Predicting the endpoints of earthquake ruptures. *Nature* 444 (7117), 358-260.

Zhang, X., Glennie, C., & Kusari, A., 2015. Change detection from differential airborne LiDAR using a weighted anisotropic iterative closest point algorithm. *IEEE Journal of Selected Topics in Applied Earth Observations and Remote Sensing* 8 (7), 3338-3346.

Zhang, H., Koper, K. D., Pankow, K., & Ge, Z., 2017. Imaging the 2016 M_w 7.8 Kaikoura, New Zealand Earthquake with Teleseismic P Waves: A Cascading Rupture Across Multiple Faults. *Geophysical Research Letters* 44, 4790–4798.